Journal of Alloys and Compounds 615 (2014) S515–S521

Contents lists available at ScienceDirect

Journal of Alloys and Compounds

journal homepage: www.elsevier.com/locate/jalcom

Chitosan and chitosan composites reinforced with carbon nanostructures

C.N. Brysch [a], E. Wold [a], M. Patterson [a], R. Ordoñez Olivares [b], J.F. Eberth [c], F.C. Robles Hernandez [a,*]

[a] Department of Mechanical Engineering Technology, University of Houston, Houston, TX 77204-4020, USA
[b] Mechanical Engineering and Materials Science Department, University of Pittsburgh, Pittsburgh, PA 15261, USA
[c] Cell Biology and Anatomy, University of South Carolina School of Medicine, Columbia, SC 29208, USA

ARTICLE INFO

Article history:
Available online 18 January 2014

Keywords:
Composite materials
Powder metallurgy
Crystal structure
Grain boundaries
Mechanical properties
Thermal analysis

ABSTRACT

Chitosan is a naturally-occurring polymer that can be derived from chitin through a deacetylation process from shells of crustaceans. Chitosan is abundant, easily collected as waste and repurposed for industrial and biomedical applications. This work demonstrates that the mechanical properties of chitosan can be improved by thermomechanical processing (milling and sintering) and through reinforcement with carbon nanostructures (CNS) to form mechanically tunable composites. Thermal analysis was used to optimize the sintering conditions for chitosan and chitosan–CNS preventing unwelcome degradation. The crystallinity index (CI%), ratio among crystalline (β) and amorphous (α) phases, decreases from 57 to 18 depending on milling and sintering conditions. Although, the crystalline structure is affected during processing, Raman results demonstrated that the chitosan bonding is preserved and the added CNS percolate the chitosan. Pressing chitosan at room temperature does not guarantee consolidation, while chitosan sintered at 180 °C can reach a hardness of up to 15 ± 0.7 μHV. Addition of CNS and sintering at 220 °C demonstrate further benefits on hardness (26.1 ± 0.1 μHV) this hardness improvement is attributed to a grain boundary reduction and improved cohesion among chitosan and CNS. The nanohardness testing shows a unique elastic phenomenon resulting from the presence of graphene or graphitic carbon in the CNS.

Published by Elsevier B.V.

1. Introduction

The development of multi-functional bio-composites is a topic of great interest in material science and bioengineering [1,2]. Low procurement and low production cost material are especially desirable as engineering materials with a great emphasis on recycled waste. Chitosan is one such tunable material that offers both bio-compatibility and can be reinforced with carbon nanotubes, graphenes, and other carbon species [3]. Researchers have demonstrated that carbon nanostructures (CNS), namely carbon soot, are effective reinforcements for structural applications [4–7]. Furthermore, the properties of chitosan can be improved by sintering or heat treatments under the right conditions.

Mechanical milling produces highly homogeneous nanostructured materials, improves integrity and has positive effects on mechanical properties [8,9]. The nature of high energy mechanical milling allows for the manufacture of highly homogeneous composites in short times. This is attributed to the enhancing the level of intimacy among the constituents. Conventional sintering, the process of consolidate powders, is proposed to preserve the delicate nature of chitosan while improving upon the material properties. The sintering process can be evaluated and quantified using thermal analysis; an accepted method to determine precise phase transformations in structural materials [10–12] and animal tissue [13].

In this work we demonstrate that reinforcement of chitosan with CNS has improved mechanical properties compared to that of controls. We propose a methodology to produce and tune these homogeneous chitosan–CNS composites. The proposed methodology is carried-out by well-known methods such as mechanical milling, and sintering. The material was characterized and tested in order to demonstrate its advantages of pressed and sintered chitosan with those of the sintered composites.

2. Methods

Samples were prepared using 80% deactylated chitosan (Carbomer Inc., San Diego CA) and commercially available fullerene soot (SES Research, Houston TX). Mechanical milling was conducted on a SPEX apparatus for 6 and 30 h for the chitosan and 3 h for the fullerene soot. The chitosan–CNS composite samples were mixed at a 98:2 weight ratio (chitosan–CNS) and milled together for an additional 1.5 h. The sintering was performed on a custom made French press-heater (Fig. 1).

* Corresponding author.
E-mail address: fcrobles@uh.edu (F.C. Robles Hernandez).

http://dx.doi.org/10.1016/j.jallcom.2014.01.049
0925-8388/Published by Elsevier B.V.

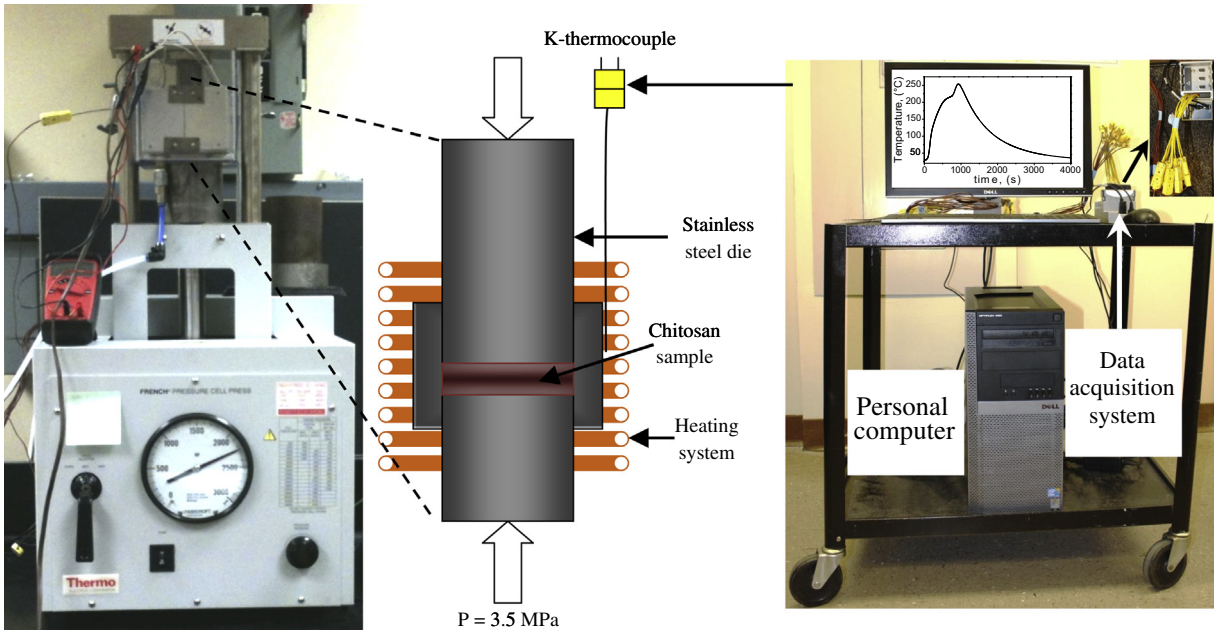

Fig. 1. (Left) French-press and custom designed heater system used to sinter chitosan and chitosan–CNS samples (Center) heater and die demonstrated in pictorial form. (Right) PC-based-DAQ thermal analysis system.

The temperature was monitored via high speed, high resolution data acquisition system (NIcDAQ-9174: National Instruments, Austin TX) as shown in Fig. 1. The same system was used to collect the data for thermal analysis, but this process was carried in a tube furnace. The sintering was conducted at 180 and 220 °C for 3 and 12 h under a constant pressure of 3.5 MPa through the entire sintering process. All experiments were carried out in a helium atmosphere. The temperature during sintering was measured in close proximity to the die (see Fig. 1). Through calibration of the equipment, we determined that the sintering temperature can be up to 30 °C lower to that measured by the thermocouple. We used this temperature to offset the collected data.

Hardness testing was performed on all samples using micro and nanohardness methods. For microhardness we used the Vickers method on a M-400-G Lecco apparatus with a load of 150 g–f and dwelling time of 10 s. The nanohardness was performed in a Hysitron TI-900 TriboIndenter™ system with real-time data collection. The reported values are the average of 6 measurements. The applied load was 1000 μN. The system has a 1 nN and 0.0004 nm resolution in loading and displacement respectively. X-ray diffraction (XRD) was measured with a D5000 SIEMENS diffractometer at $K\alpha$ = 0.15406 nm. The crystallinity index is determined based on the expression: $CI\% = [(I_{110} - I_{am})/I_{110}] \times 100$ where CI% is the crystallinity index, I_{110} the intensity (arbitrary units) of the reflection (110) for the β-phase and I_{am} the intensity of the amorphous phase (α) [14,15]. The presence of the α-phase is not possible by the use of a similar XRD expression. The SEM observations were carried out on a FEI XL-30FEG on secondary electrons. Finally, a Raman analysis was done on a confocal micro-Raman microscope XploRA™, Horiba JY. A 638 nm diode laser was used for excitation.

3. Results

SEM and XRD characterization of the raw materials are shown in Fig. 2. The SEM image of chitosan shows a chunky structure with a regular distribution of particles of various sizes. The XRD results indicate that chitosan has a defined crystalline structure and matches that previously reported in the literature [16]. The XRD results suggest that chitosan is composed of both, α and β, phases with a crystallinity index of 57. The fullerene soot is characterized by the fluffy appearance (Fig. 2c). Fig. 2b shows the presence of fullerene and a short range ordered phase (identified as $(002)_{Gr}$), characteristic of the basal plane of graphite. The fullerene soot is the byproduct, leftover, after the recovery of fullerene produced by the Kratschmer method [17]. Fullerene is expected since the soot is the byproduct after the fullerene removed. The supplier indicates that fullerene is present on traces and no more than 1 wt% is present in the soot that is in agreement with the observations.

Fig. 2d shows an integrated Raman spectrum of the fullerene soot with bands of C_{60}; one fundamental and one second-order combinational identified at 710 cm^{-1} ($H_g(3)$) and at 2898 cm^{-1} ($A_g(2)+H_g(7)$), respectively [18]. The other Raman bands of C_{60} are weaker and they may be hidden under the G and D bands of graphitic carbon. The main Raman bands are D, G and 2D bands of graphitic (sp^2) carbon at 1318 cm^{-1}, 1578 cm^{-1}, and 2660 cm^{-1}, respectively. Graphitic carbon may also contribute to the band at 2898 cm^{-1} through the D + G two-phonon scattering channel. The estimated average lateral size of graphitic particles is 40 nm as determined using the expression reported [19].

Fig. 3 shows the heating/cooling and first derivative of temperature with respect to time for the raw chitosan (80% deacetylation). The heating/cooling curve demonstrates the presence of phase transformations. The optimal sintering temperature is near, but below the degradation temperature. Temperatures above degradation damage the chitosan permanently with negative consequences for sintering. This deterioration is observed in Fig. 3b by the exothermic reaction (likely burning) taking place above 215 °C and it is confirmed by the discoloring ashy appearance of the loose material. Based on the collected information we used the criteria that sintering temperature (T_S) should be conducted at $T_S = (0.8–0.9)\cdot T_T$, where T_T is the transformation (in this case degradation) temperature in *K*. These conditions were set to guarantee that the minimum activation energy requirement for sintering are met at temperatures below degradation to reduce sintering time [20]. The approximate weight loss in the sample seen in Fig. 3c and d are 12% and 30% in weight respectively.

The XRD results are presented in Fig. 4 for the sintered samples at 180 °C and 220 °C. Both figures demonstrate that milling time lowers the crystallinity index. It is also observed that the presence of CNS slightly reduced the CI%. The major contributor to the reduction of the CI% seems to be the sintering time. This effect is observed by the enhancement of the α phase of chitosan that is also known as the amorphous phase. The samples milled for 6 h have comparable CI% except for that one sintered for 12 h that has the lowest CI% of 20 suggesting that sintering time has a more a negative effect on crystallinity than milling time.

Raman characterization was conducted to observe the effects of milling and sintering on chitosan and to show the effects of carbon

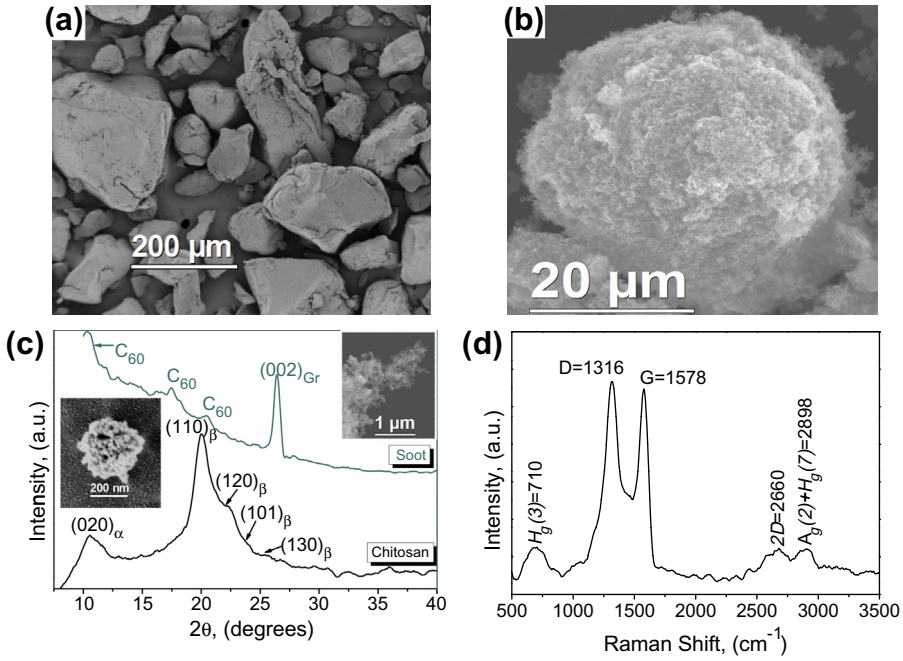

Fig. 2. Characterization of the raw (a and c) chitosan and (b and c) soot by means of (a and b) scanning electron microscopy and (c) X-ray diffraction.

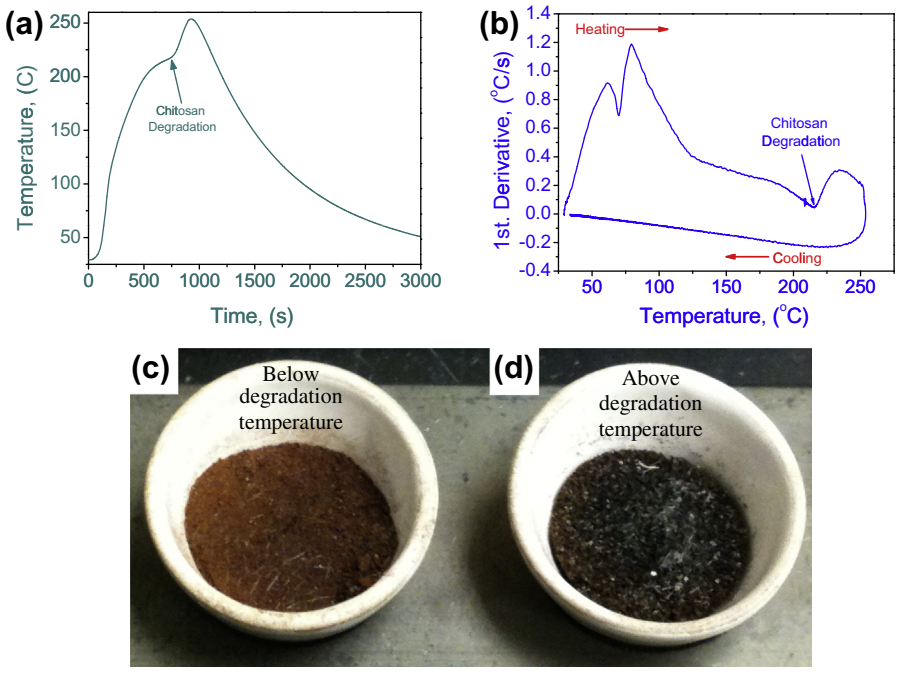

Fig. 3. (a) Heating/cooling curve for chitosan and (b) the first derivative of the heating/cooling curve. Samples of chitosan before (c-left) and after (d-right) the degradation temperature.

nanostructures on the composites in powdered and sintered forms. The analysis conducted in bulk (100× magnification) on the powders, sintered chitosan and sintered chitosan–CNS composite are almost identical (Fig. 5). At this magnification Raman active bands in the powder as well as the composites before and after sintering can be identified. At 1087 cm^{-1} the skeletal vibration C–O stretching generally related to the saccharide structure typical of chitosan. The anti-simetric C–O–C bridge is the band observed at 1154 cm^{-1} and it is indicated with a B. The identification of the Raman bands correspond to the C–H bending at approximately 1381 and 1423 cm^{-1} and are identified as C and E in Fig. 5 respectively. The N–H bending mode is typically found at 1598 cm^{-1} and corresponds to the primary amine group (letter F).

From Fig. 5 it is evident that magnification makes a difference in the Raman analysis. Using a magnification of 1000× the Raman analysis goes from bulk to discrete allowing a clear identification of the carbon in the chitosan–CNS composite. Fullerene is not identified by Raman in the composite because its presence is in parts per millions compromising its detection. The carbon CNS are identified by the G and D bands. These are the two most common bands of carbon. The G band is also called the graphite band and related to graphitic bonding (sp2). On the other hand the D band is the

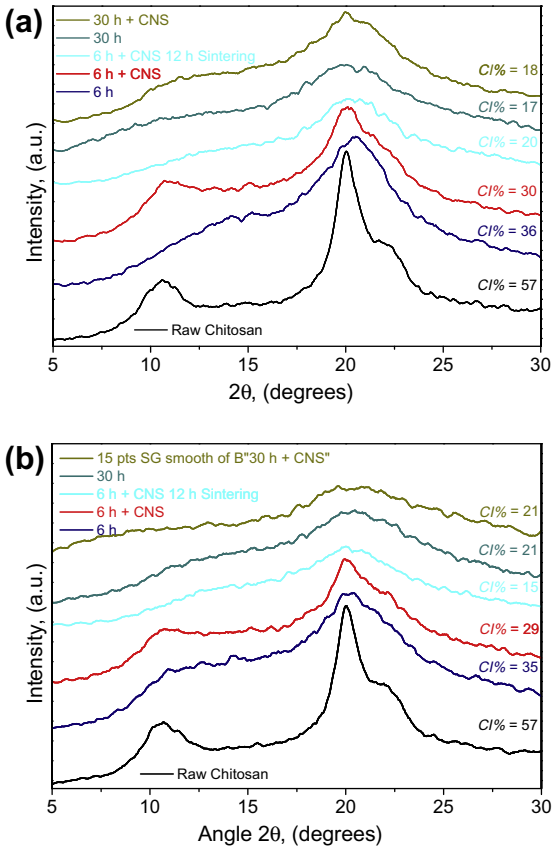

Fig. 4. XRD results of sintered chitosan and chitosan–CNS composites sintered at (a) 180 °C and (b) 220 °C. CI% stands for the cystallinity index. All samples were sintered for three hours except for the raw chitosan that was only pressed during sintering and a sample that was sintered for 12 h.

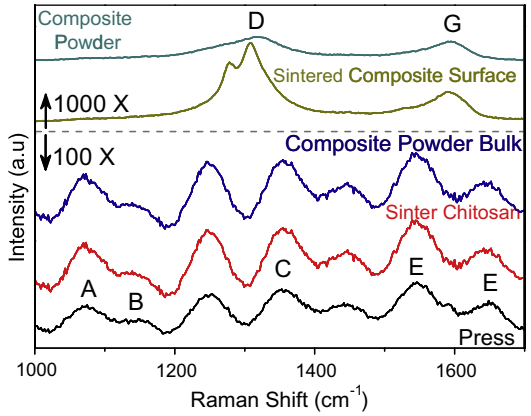

Fig. 5. Raman analysis of the chitosan and chitosan–CNS composites. Notice the significant differences in the Raman spectra at the different magnifications used in the present work. *Note*: the following samples were observed at 100×: chitosan, sinter chitosan and composite powder; while a 1000× magnification was used for the composites (sintered and powder).

defect band that is usually active in nanostructured graphitic particles as previously identified in [4]. Due to the relative intensity among the D and the G bands it can be concluded that the carbon used in this work has a graphitic nature with a high density of defects. The D band should not be confused with the diamond band that has a narrow and sharp band at 1334 cm^{-1} [21]. Using higher magnification it is possible to observe the carbon nanostructures implying that they are located at the surface of the chitosan particles making proper cohesion within in the composite.

Fig. 6a and b shows micrographs of the powders before and after milling. The powder before milling is composed of particles of approximately 50 μm or larger. After milling the powders agglomerate into clusters that are carbon coated along their surface. Pictures of the sintered samples are given in Fig. 6c–e. The change in color in the composites is attributed to the carbon additions. The chitosan has an off-white color while sintering results in a browning of the material. The chitosan–CNS composites are highly homogeneous as shown by their consistent dark color at only 2 wt% of added CNS. HRTEM images of the CNS are presented in Fig. 6f and g. Those figures show that the CNS have graphitic nature with interatomic distance of 0.34 nm similar to that on graphene [4,7,22]. The crystal size of the graphitc particles is about 40 nm as calculated in our previous work [4,7].

Fig. 7 shows optical micrographs of chitosan and chitosan–CNS composites. In Fig. 7a the compacted chitosan and Fig. 7d the chitosan–CNS composite sintered at 180 °C. In the chitosan samples the grain boundaries are wider than those in the sintered samples. This results from the expected low cohesion among the chitosan particles that is improved with the sintering conditions and CNS additions. The grain boundaries in the chitosan–CNS composite are relatively difficult to identify; although, some porosity is still present, but in lower amounts and smaller sizes. In the higher magnification images, it is possible to visualize the grain boundary and the effect of temperature and carbon in the chitosan–CNS composite. The arrows in Fig. 7c–f are used to indicate the grain boundary. In the chitosan sintered samples, this gap is 2–4 μm range. In the case of the chitosan–CNS composite the gaps is sub-micrometric (1–2 orders of magnitude smaller).

Table 1 summarizes the microhardness testing results of the chitosan and the chitosan–CNS composites. The chitosan samples show the lowest hardness in particular when they are sintered at 180 °C. When the chitosan samples are sintered to 220 °C the hardness increases. However larger milling times (30 h) seem to have a negative effect on hardness. The contrary is observed with the addition of CNS. A direct comparison among the hardness in the chitosan sintered samples with that in the composites show improvements of 14–15% for the samples sintered at 180 °C and only 13% difference when sintered at 220 °C. Sintering for 12 h compared to 3 h does not seem to affect hardness. The consistency of the pressed sample without sintering is so delicate and weak that hardness measurements were not possible. Therefore if we compared the results with that sample we can conclude that the composite has appreciably higher mechanical properties.

Fig. 8 shows the results of nanohardness for the chitosan and chitosan–CNS composites. The respective hardness values are 265 and 287 MPa that represent an 8% improvement. The elastic modulii are 7.0 and 2.1 GPa that correspond to a 73% increase in the chitosan sample. The recovery for the chitosan is 42% while the recovery for the composite is 72%. This recovery and elastic deformation observed in the composite is unique and is directly attributed to the additions of CNS. The nanohardness indentations were resolved by the scanning system in the chitosan, but were not observed in the chitosan composite. This phenomena is attributed to the elastic behavior resulting from the CNS that allows for a better recovery of the composite. The grain boundary in the chitosan sample is larger than that of the composite confirming the results presented in Fig. 7.

4. Discussion

Thermal analysis is an effective method to control the phase transformations occurring during the heating of chitosan. These

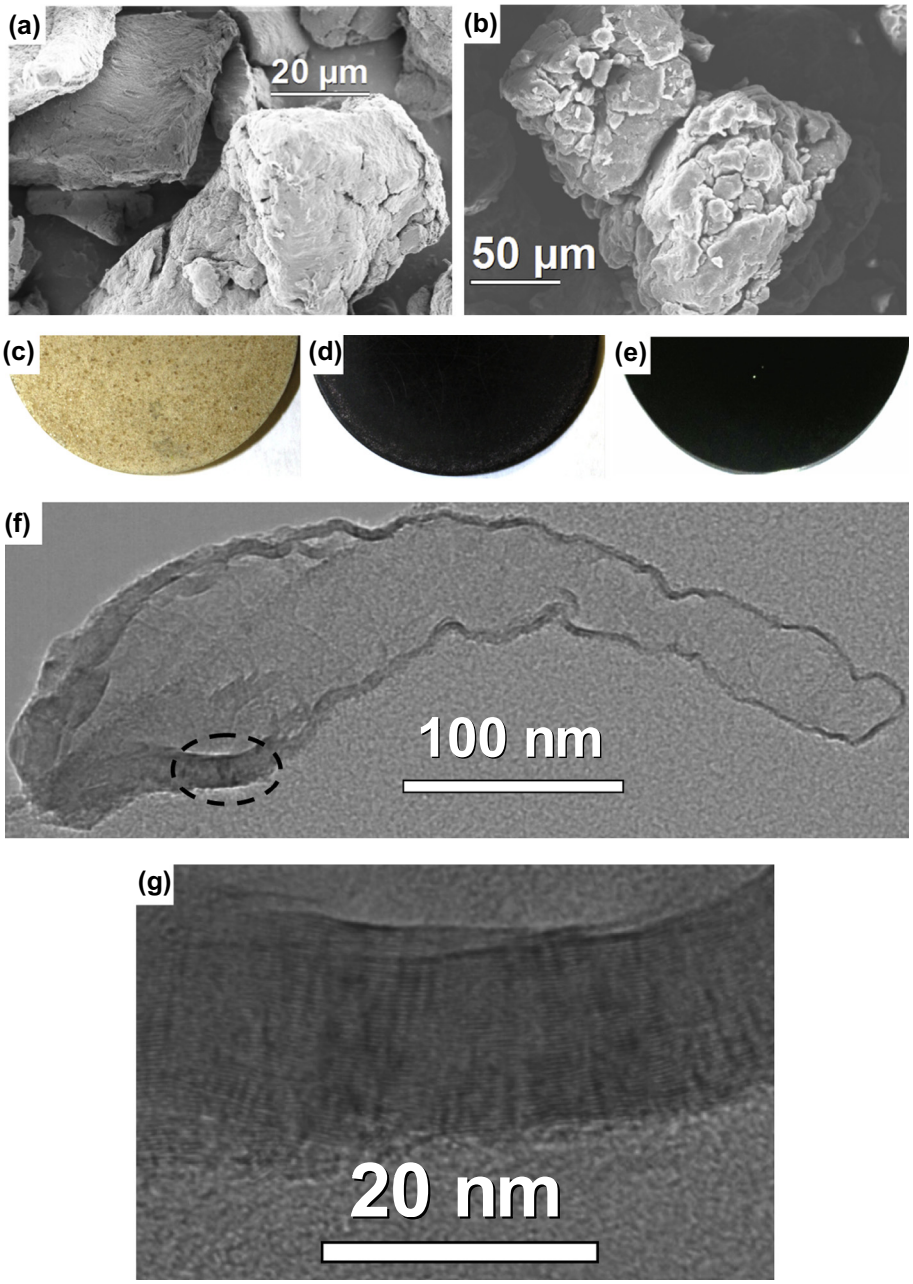

Fig. 6. Scanning electron micrographs of the (a) chitosan powders (b) the chitosan–CNS composite milled for 6 h. Sintered samples at 180 °C of (c) chitosan, (d) chitosan–CNS composite and (e) chitosan–CNS composite sintered at 220 °C. *Note*: the diameter of the sintered samples is 25.4 mm. HRTEM images are presented in (f and g); micrograph in (g) corresponds to the encircled area in (f) at higher magnification to depict the graphitic nature of the CNS having a d-spacing of 0.34 nm.

phase transformations have distinct heat transfer characteristics as indicated by the change in slope of the heating/cooling curves. The first derivative of temperature with respect to time vs. temperature not only determines the transformations but the level of reversibility of the sample as well. The algorithms reported in [11,13] were designed to determine the fraction of the material that is changing phase or "fraction transforming". Heating an organic material above the degradation temperature decomposes it; such phenomenon is presented in Fig. 3a and b. The irreversibility, in this case, is attributed to the burning of chitosan. Therefore, proper sintering of chitosan must be conducted at temperatures close, but below, degradation.

Comparing Figs. 3–5 it can be observed that after the degradation temperature chitosan transforms to ashes. On the other hand mechanical milling affects the crystallinity of chitosan as seen from the XRD results. This does not imply that the bonding structure is affected; in fact, the Raman results of before and after the milling are identical. Nonetheless, the microhardness of the samples is negatively affected up to 20%.

Mechanical milling is an effective method to refine the grain structure of chitosan and it helps to develop an even distribution of particle sizes. Additionally, it allows the proper formation of a composite by dispersing the CNS homogeneously. This can be confirmed by the uniform change in coloration. This in turn allows a better sintering potential as shown in Figs. 6 and 7 and further confirmed by the improvements in hardness shown in Table 1. The ultimate contributor to the integrity and consistency of the composite is the presence of CNS. However, at the nanoscale the composite

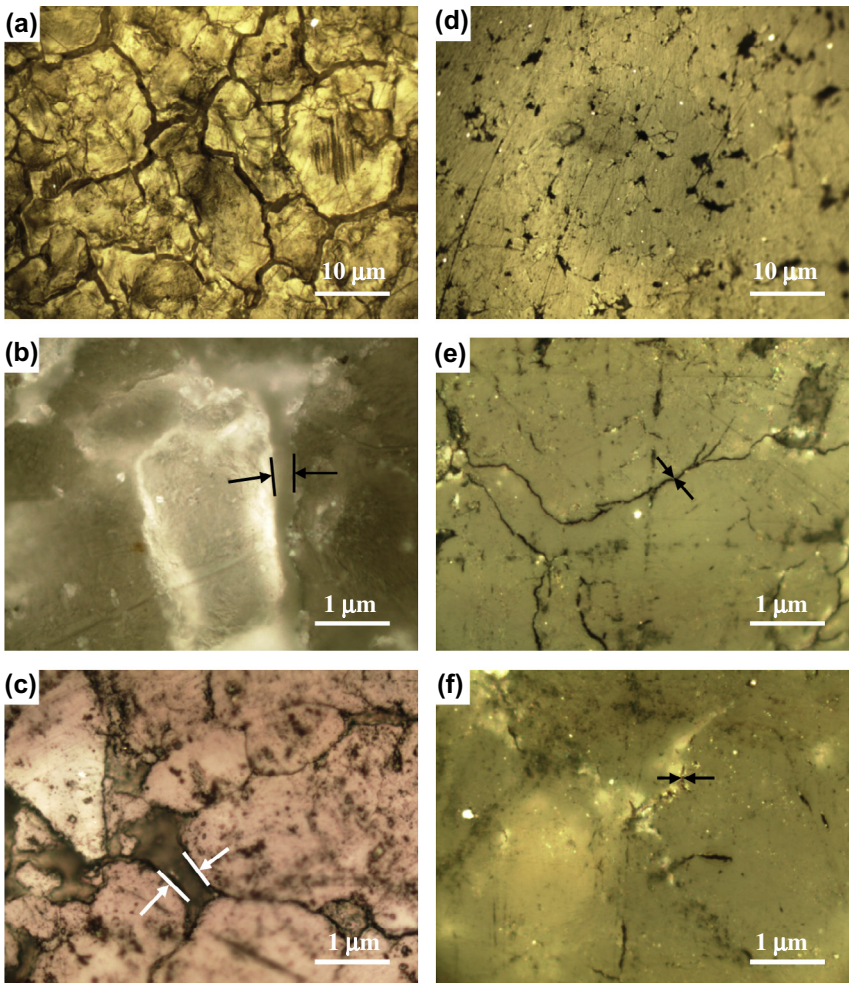

Fig. 7. Optical characterization of the (a–c) chitosan samples and (d–f) chitosan–CNS composites. Sample (a) was compacted at room temperature, samples (b–f) are the sintered samples. The sintered samples at 180 °C are (b–e) and the samples sintered at 220 °C are (c and f). All micrographs correspond to a sintering under a constant pressure of 3.5 MPa for 3 h. Arrows are used to indicate the gaps along the grain boundary.

Table 1
Microhardness testing of the chitosan and chitosan–CNS composites sintered at 180 and 220 °C for 3 h except where indicated. The samples were sintered using a 3.5 MPa of constant loading. Hardness values in μHV.

Sample	Microhardness (μHV)	
	180 °C	220 °C
Chitosan		
Milling 6 h	18.4 ± 5.4	23.1 ± 1.6
Milling 30 h	15.1 ± 0.7	23.6 ± 0.1
Chitosan–CNS composite		
Milling 6 h	21.2 ± 2.5	26.1 ± 2.7
Milling 30 h	17.6 ± 1.8	24.1 ± 0.6
		26.2 ± 0.8[a]

[a] Sample sintered for 12 h.

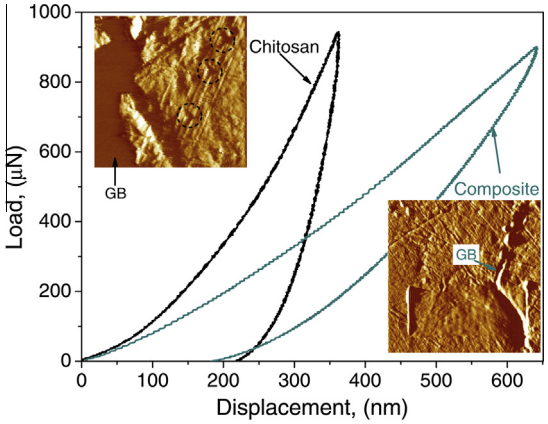

Fig. 8. Nanohardness results for the chitosan and chitosan–CNS composites milled for 6 h, and sintered for 3 h at 220 °C. The insets are tapping mode images from the nanoindentor, in the chitosan samples the dotted circles are used to identify the Berkovich impressions. *Note*: the Berkovich impressions in the chitosan–CNS composite were not identified.

does not seem to have significant improvements on hardness; nonetheless, the elastic characteristics of the composite improve significantly (Fig. 8) allowing an almost full recovery of the material. Further, this prevents the proper observation of the indentation. It is of interest that only 2 wt% of CNS is sufficient to have such improvements in mechanical properties. The elastic modulii, hardness, and recovery of the composite presented herein are superior to those previously reported in composites reinforced with nanotubes [23] and uncrossed-linked chitosan [24]. We attribute this elastic behavior to the graphitic nature observed in the CNS as seen in Fig. 5.

The single layer graphene had reported outstanding elastic behavior [25] and self-healing mechanisms numerically [26] and experimentally [27]. Both mechanisms may be responsible for

the elastic properties observed in the investigated composites. The graphitic nature of the CNS used in this work was reported in our previous work [4,7], which in this work is observed in the XRD and Raman results (Figs. 2 and 5) presented herein.

5. Conclusions

Thermal analysis is an accurate tool to precisely predict the sintering temperature which is both critical to achieve the best characteristics in the composite. Temperature improves the sintering effectiveness by reducing grain boundaries and porosity that in turn results in better intimacy among the constituents in the composite. Still, the use of CNS is more effective to improve hardness and most importantly the elastic behavior of the composite. This elastic behavior is attributed to the graphitic carbon present in the CNS and the recovery to a self-healing mechanism. The CNS enhances the intimacy among the constituents of the composite resulting in superior mechanical behavior. The elastic behavior has not been reported yet and is largely attributed to the graphitic nature of the CNS.

Acknowledgments

The authors would like to acknowledge the contributions of undergraduate researcher Alexandra Ulmet. FCRH would like to express his gratitude to the University of Houston and the State of Texas Higher Education Assistance Fundis (HEAF).

References

[1] M. Dash, F. Chiellini, R.M. Ottenbrite, E. Chiellini, Prog. Polym. Sci. 36 (2011) 981–1014.
[2] H.L. Fan, L.L. Wang, K.K. Zhao, N. Li, Z.J. Shi, Z.G. Ge, Z.X. Jin, Biomacromolecules 11 (2010) 2345–2351.
[3] J. Venkatesan, S.K. Kim, Mar. Drugs 8 (2010) 2252–2266.
[4] A.E. Fals, V.G. Hadjiev, F.C. Robles Hernández, Mater. Sci. Eng.: A 558 (2012) 13–20.
[5] V. Garibay-Febles, H.A. Calderon, F.C. Robles-Hernadez, M. Umemoto, K. Masuyama, J.G. Cabanas-Moreno, Mater. Manuf. Process 15 (2000) 547–567.
[6] I. Santana-García, F. Hernandez-Robles, V. Garibay-Febles, H. Calderon, Microsc. Microanal. 10 (2010) 2.
[7] A.E. Fals, V.G. Hadjiev, F.C. Robles Hernández 140 (2013) 651–658.
[8] P.S. Gilman, J.S. Benjamin, Annu. Rev. Mater. Sci. 13 (1983) 279–300.
[9] C. Suryanarayana, Prog. Mater. Sci. 46 (2001) 1–184.
[10] A. Mitrasinovic, F.C. Robles Hernández, M. Djurdjevic, J.H. Sokolowski, Mater. Sci. Eng. A 428 (2006) 41–46.
[11] F.C. Robles Hernandez, J.H. Sokolowski, J. Alloys Comp. 419 (2006) 180–190.
[12] F.C. Robles Hernández, J.H. Sokolowski, Adv. Eng. Mater. 7 (2005) 1037–1043.
[13] F.C. Robles Hernandez, J.A. Neal, U.S. Aldea, J. Food Process Eng. 36 (2013) 160–172.
[14] J. Kumirska, M. Czerwicka, Z. Kaczynski, A. Bychowska, K. Brzozowski, J. Thoming, P. Stepnowski, Mar. Drugs 8 (2010) 1567–1636.
[15] B. Focher, P.L. Beltrame, A. Naggi, G. Torri, Carbohyd. Polym. 12 (1990) 405–418.
[16] I.S. Lima, C. Airoldi, Thermochim. Acta 421 (2004) 133–139.
[17] W. Kratschmer, L.D. Lamb, K. Fostiropoulos, D.R. Huffman, Nature 347 (1990) 354–358.
[18] Z.H. Dong, P. Zhou, J.M. Holden, P.C. Eklund, M.S. Dresselhaus, G. Dresselhaus, Phys. Rev. B 48 (1993) 2862–2865.
[19] L.G. Cançado, K. Takai, T. Enoki, M. Endo, Y.A. Kim, H. Mizusaki, A. Jorio, L.N. Coelho, R. Magalhães-Paniago, M.A. Pimenta, Appl. Phys. Lett. 88 (2006).
[20] S.-J.L. Kang, Sintering Densification, Grain Growth and Microstructure, in, Butterworth-Heinemann [Imprint], Elsevier Science & Technology Books, San Diego, 2005. p. 280.
[21] A.C. Ferrari, J. Robertson, Phys. Rev. B 63 (2001).
[22] J.R. Jinschek, E. Yucelen, H.A. Calderon, B. Freitag, Carbon 49 (2011) 556–562.
[23] S.F. Wang, L. Shen, W.D. Zhang, Y.J. Tong, Biomacromolecules 6 (2005) 3067–3072.
[24] A. Aryaei, A.H. Jayatissa, A.C. Jayasuriya, J. Mech. Behav. Biomed. 5 (2012) 82–89.
[25] C. Lee, X.D. Wei, J.W. Kysar, J. Hone, Science 321 (2008) 385–388.
[26] L. Tsetseris, S.T. Pantelides, Carbon 47 (2009) 901–908.
[27] Y.X. Xu, Q.O. Wu, Y.Q. Sun, H. Bai, G.Q. Shi, Acs. Nano 4 (2010) 7358–7362.